Journal Name

ARTICLE

Helium stability and its interaction with H in α-Al_2O_3: A first-principles study

Received 00th January 20xx,
Accepted 00th January 20xx

DOI: 10.1039/x0xx00000x

www.rsc.org/

Guikai Zhang, Xin Xiang, Feilong Yang, Xuexing Peng, Tao Tang, Yan Shi, Xiaolin Wang*

Little is known about hydrogen interaction with helium, an extrinsic defect, presenting in α-Al_2O_3 TPBs due to tritium decay and (n, a) reaction. Using density functional theory (DFT), the stability, structure and diffusion of He-related complex at the different positions (V_{Al}^{3-}, V_O^0, O_i^{2-} and octahedral interstitial site (OIS)) in α-Al_2O_3, as well as the interactions with H are determined under H_2-rich condition. He atom favors to occupy Al vacancies, centers of OIS or form a dumbbell around Al vacancies, forming He_i, He_{Al}^{3-}, He_i-He_{Al}^{3-}, $[V_O^0\text{-}He_i]^0$ and $[O_i^{2-}\text{-He}]^{2-}$ complexes, among of which He_{Al}^{3-} forms most readily. The V_{Al}^{3-} can attract He to form small stable He-He_{Al}^{3-} clusters, whereas only a He atom trapped by OIS, V_O^0 and O_i^{2-}. He_i is more likely diffusion into V_{Al}^{3-} and V_O^0 than the diffusion along the c axis from one OSI to another. H_i^+ trapping into the He_{Al}^{3-} and $[V_O^0\text{-}He_i]^0$ are thermodynamically and kinetically feasible, whereas dissociation of $[He_i\text{-}H^+]^+$ is more feasible. Forms of H-He complex defect in α-Al_2O_3 are He_i, H_i^+, $[He_i\text{-}H^+]^+$, $[He_{Al}^{3-}\text{-}H^+]^{2-}$ and $[H_O^+\text{-}He_i]^+$. He_{Al}^{3-} and $[V_O^0\text{-}He_i]^0$ presenting will increase the activation energy of H migration in α-Al_2O_3, which is favored for low H-transport of TPBs.

1. Introduction

Various oxide materials, such as Al_2O_3, Y_2O_3, ZrO_2 and so on, are used in fusion reactors as plasma diagnosis windows, electric insulators, oxide dispersion-strengthened (ODS) ferritic steels and tritium permeation barrier (TPB) [1]. The use of TPB of α-Al_2O_3, due to its chemical stabilities and low solubility for hydrogen, on structural material is efficacious way to suppression of hydrogen isotopic permeation through steel wall of duct for hydrogen storage & distribution, hydrogen embrittlement protection and control of the tritium inventory in future fusion reactors like ITER [2, 3].

The effectiveness of TPBs depends critically on the thermodynamics and kinetics of hydrogen transport within the barrier materials [2–4]. It has been proposed that properties of metal oxide materials are directly or indirectly connected to the presence of defects, such as vacancies, impurity, dislocations and grain boundaries [3, 5]. However, to the authors' knowledge, interactions between hydrogen and defects in α-Al_2O_3, and their effect on the thermodynamics and kinetics of the H-mass transport within α-Al_2O_3 have not been studied well.

Helium impurity, an extrinsic defect, presents in TPBs due to tritium decay and (n, a) reaction. It is currently accepted that the presence and migration of helium can have a strong influence on microstructural and physical properties of natural or manufactured inorganic solids, thus a deep knowledge of the physical mechanisms of helium is required [6]. Furthermore, a deep knowledge of the physical mechanisms of deuterium, tritium and helium and their synergy determining the long-term stability of the selected materials is required, assessing long-term predictions of the behaviours of operating components in fusion reactors [3].

For intrinsic defects of α-Al_2O_3, studies previously addressed that fully ionized states of V_{Al}^{3-}, V_O^{2+}, Al_i^{3+}, O_i^{2-} and Schottky defects ($2V_{Al}^{3-}$-$3V_O^{2+}$) are energetically favorable in α-Al_2O_3 under O-rich conditions[7]. However, we recently find that the most stable Schottky defect is not the common considered ($2V_{Al}^{3-}$-$3V_O^{2+}$), and the most stable defect is Frenkel defect (O_i^{1+}-V_O^{1-}). The relative stability is in the order of Schottky > Al Frenkel > O Frenkel > antisite defect[8]. For intrinsic defects interacting with hydrogen, interstitial H in α-Al_2O_3 has been assigned to the neutral charge state (H_i^0) by theoretical works for over decades, occupying an octahedral site in the Al sublattice of α-Al_2O_3 [9, 10]. Up to 2013, Aaron M Holder reported that the neutral charge state H is never the most stable form in α-Al_2O_3 and negatively charged hydrogenated Al cation vacancies likely form[11]. We found that the stable forms of H related defect in α-Al_2O_3 are charged H interstitials (H_i^q, q is charge state of defect) and hydrogenation of the bulk V_{Al}^{3-} ($[V_{Al}^{3-}\text{-}H^+]^q$), under hydrogen-rich conditions. As the system reaches equilibrium, H in α-Al_2O_3 is in present of H_i^+ state mainly, and like to exist in the form of $[V_{Al}^{3-}\text{-}H^+]$ and Ho^+. H_i^+ is the predominant diffusion species in α-Al_2O_3, $[V_{Al}^{3-}\text{-}H^+]$ and H_O^+ are more stable than HO_i^- and can release trapped hydrogen during high temperature annealing, contributing to the H-transport into α-Al_2O_3 [12].

Institute of Materials, China Academy of Engineering Physics, 621908, Jiangyou, China. E-mail: xlwang@caep.cn; Tel: +86 81636 26481.

Contrary to these, thermodynamic and kinetic information (i.e. defect formation energies, migration barriers, etc.) for extrinsic defect of helium, further their roles in thermodynamics and kinetics of the H-mass in α-Al_2O_3, is considerably inferior. Few groups have already been carrying out experimental and theatrical works of helium diffusion in α-Al_2O_3 [13, 14]. Especially, theoretical works on helium migration in non-metallic materials remain much less common than those devoted to metallic materials[6]. The main reason comes from the fact that non-metallic compounds contain at least two or more kinds of atoms with their own structural properties and electronic configurations, leading to a huge number of specific interactions between them within the network to be used as inputs in the model. Theoretical works suggest that three main mechanisms are relevant to describe helium diffusion in non-metallic materials: interstitial mechanism, vacancy mechanism and a mechanism in which an interstitial atom displaces an atom from its normal substitutional site, and then the substitutional atom moves to a free interstitial site[6]. The major physical mechanisms able to affect helium migration are trapping/detrapping processes by/from point or extended defects, interactions with grain boundaries, and growth of bubbles.

In present study, using density functional theory, the relative stability, structure and diffusion of He-related complex at different positions available in α-Al_2O_3 are determined under TPB working conditions, as well as the interactions with H. These results will be useful data not only to understand the physical interaction of helium with hydrogen in oxide-materials and parameterize multi-scale models of the kinetics of helium and hydrogen for nuclear reactor environments, but to understand the anti-irradiation properties of the oxide particles in ODS steels.

2. Computational method and model

We utilize DMol3[15] program package in Materials Studio of Accelrys Inc to carry out first principles total energy calculations in the PW91-GGA[16]. We adapt the double numerical quality basis set (DNP) with polarization functions[17] and the all-electron[18]. The convergence criteria were the same as those in Ref. 12 performed on bulk α-Al_2O_3 with the charged defects, giving energies computationally converging to within 2 meV/atom, which is sufficient to converge our results. All calculations, without spin polarization, utilize a convergence tolerance of energy of 1.0×10^{-5} Ha/atom (1 Ha =27.211 eV), a maximum force of 0.002 Ha/Å, a maximum displacement of 0.005 Å and a real-space cutoff of 4.3 Å.

DFT-GGA does not explicitly account for Van der Waals interactions, thus, the isolated He-He interaction energy has been tested at a range of interatomic distances from 0.15 to 0.35 nm and compared with full configuration interactions (CI) [19] and quantum Monte Carlo (QMC) simulations[20] which do include Van der Waals interactions. The GGA from PW91 shows the best agreement (Fig.1) with the CI and QMC simulations with the largest absolute difference being 0.02 eV and thus, the method of PW91 has been used for describing the exchange correlation effects with confidence that DMol3 can appropriately reproduce the behavior of helium.

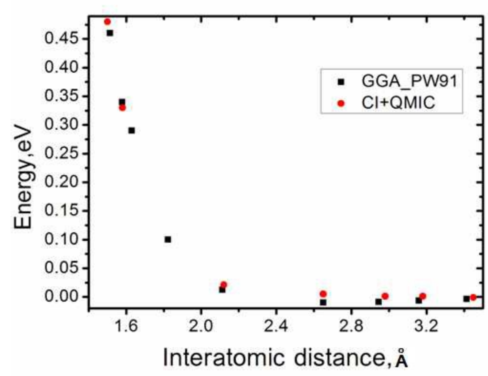

Fig. 1. Comparison of the interaction energy of a helium dimmer in the ranges of 0.15 and 0.35 nm with CI[19] and QMC[20] data using potentials from PW91 as implemented in DMol3.

To calculate defect-behaviours, the 2×2×2 supercell structure (Fig.2) as that of Ref.12 was used: it consists of 240 atoms and has hexagonal symmetry. In TPB working conditions, α-Al_2O_3 usually works at 773–973 K under H_2 exposure. Such experimental condition can be considered as Al-rich annealing processes in hydrogen gas, thus, in order to determine stable sites of He-related defect under such condition, the first task was to identify the stable charged sites of intrinsic point defects in α-Al_2O_3 under H_2-rich conditions, which was previously achieved in Ref.12. It was found that negatively charged alumium-vacancy (V_{Al}^{3-}), neutral oxygen-vacancy (V_O^0) and negatively charged oxygen-interstitial (O_i^{2-}) are readily formed under H_2-rich conditions as the system reaches equilibrium. Then, possible sites for He-related complex were tested at V_{Al}^{3-}, V_O^0, O_i^{2-} and octahedral site (OIS) with introducing a He atom respectively, producing a 0.4% defect in bulk α-Al_2O_3. Second, the He-related defects interactions with H was performed by introducing a H_i^+ defect into each He-related complex, and then the migration process of H_i^+ into He-related complexes were investigated. All atoms were relaxed fully during the structure optimization and energy calculations, except for these atoms in the upper ten layers and the bottom ten layers of the supercell.

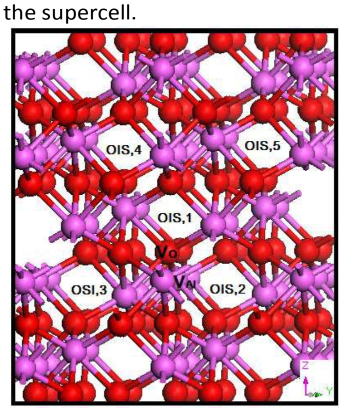

Fig.2 Side view of supercell containing 2×2×2 copies of the hexagonal unit cell of α-Al_2O_3. Red and purple balls depict oxygen and aluminum atoms. V_{Al} and V_O indicate vacancy site of aluminum and oxygen, OIS for interstitial site for oxygen, hydrogen and helium.

The relative stability of each defect has been evaluated by calculating the formation energy. Migration barriers for point defects are calculated by complete linear synchronous transit/quadratic synchronous transit (LST/QST) method using seventeen images. Frequencies are calculated at all critical points identified on the potential energy surface to identify minima and transition states, and also used to calculate zero-point energy (ZPE) corrections.

3. Results and discussion

3.1 Stability of He related defects in α-Al_2O_3

The formation energy of He-defect as,

$$E_f^{He} = E_{He-related-defect} - (E_{imperfect} + E_{He}) \quad (1)$$

, where $E_{He-related-defect}$, $E_{imperfect}$ and E_{He} are the ground state energies of the system with an helium atom present, an imperfect α-Al_2O_3 lattice and an isolated helium atom respectively. The ZPE correction is $\frac{1}{2}\sum h\omega_i$, where ω_i are the real frequencies.

Formation energies and optimized geometries of for the various positions available for helium in α-Al_2O_3 are shown in Table 1. Interestingly, He related defects have positive formation energies, denoting He related defects are less stable than the gas phase He, which suggests that He related defects form unspontaneously. The negatively charged Al-vacancy site, with forming He substitution on the Al site (He_{Al}^{3-}), has the lowest formation energy of 1.22 eV and is the most stable helium site. That is, He_{Al}^{3-} forms most readily, which could be because Al vacancy site has a large volume and low charge density[21].

Table1 Formation energy E_f, O-He distance $d_{O\text{-}He}$, Al-He distance $d_{Al\text{-}He}$ and Frequency ω for He-related defects in α-Al_2O_3, with ZPE values shown in parentheses

Configuration	He_{Al}^{3-}	He_i	$[V_O^0\text{-}He_i]^0$	$[O_i^{2-}\text{-}He]^{2-}$
E_f (eV)	1.22(0.02)	2.16(0.008)	2.07(0.008)	2.19(0.021)
$d_{O\text{-}He}$ (Å)	2.084	2.049–2.051	2.041–2.110	1.885–2.169
$d_{Al\text{-}He}$(Å)	2.571–4.779	1.918–2.021	1.949–2.029	1.949–1.954
ω(cm^{-1})	875.26, 875.75, 875.76	933.49	916.04	926.91, 901.38, 944.36

In comparison with He_{Al}^{3-}, the neutral charged oxygen-vacancy site, negatively charged oxygen-interstitial site and octahedral site are less energetically favorable site, with the forming $[V_O^0$-He], $[O_i^{2-}\text{-He}]^{2-}$ and He_i respectively. The order of the formation energies is $E_f([O_i^{2-}\text{-}He]^{2-}) > E_f(He_i) > E_f([V_O^0\text{-}He])$, however, the energy difference between these positions is very small. He_{Al}^{3-} forms most readily, quite different from H-related defects. The relative stability of H-related defects is $H_i^+ > [V_{Al}^{3-}\text{-}H^+]^{2-} > H_O^+ > HO_i^-$ [12].

In general, the constituent point defects in a complex can interact among themselves and significantly change the formation energies of certain isolated point defects. Thus, we further characterize the stability of He-related and intrinsic defects by their binding energy. The binding energy can be calculated using the formation energy of the *n*He-related complex ($n\mathrm{He}_{defect}$) and those of its constituents (*He*, (n-1)He_{defect}):

$$E_b = E_{f\ nHe_{defect}}^{He} - E_{f\ (n-1)He_{defect}}^{He} - E_{f\ He_i}^{He} \quad (2)$$

,where $n\mathrm{He}_{defect}$ and $(n\text{-}1)\mathrm{He}_{defect}$ are the α-Al_2O_3 system with *n* and *n-1* He atoms respectively. Such relation is defined that negative and positive values of binding energy respectively indicate attractive and repulsive interaction among the point defects comprising a defect complex[22].

The binding energies of the complex with *n* =2 and 3 are shown in Table 2. Once a binding energy become positive, addition of He atom did not consider further, thus binding energies of $3He_i$, $[V_O^0\text{-}3He_i]^0$ and $[O_i^{2-}\text{-}3He]^{2-}$ are not given. Moreover, binding energies of He_{Al}^{3-}, $[V_O^0\text{-}He_i]^0$ and $[O_i^{2-}\text{-}He]^{2-}$ show He interaction with intrinsic defects of α-Al_2O_3.

For perfect α-Al_2O_3, it is clearly seen that the postive binding energy between He_i and He_i signifies a repulsive interaction. However, with intrinsic point defects presenting α-Al_2O_3 lattice, the binding energy between He_i and V_{Al}^{3-} is negative for up to *n* = 2, signifying that He atom and Al vacancy tend to attract each other, that is, two He atoms will be trapped by each V_{Al}^{3-}, thus, V_{Al}^{3-} can attract He_i to form small stable He-He_{Al}^{3-} cluster.

For trapping of a He atom by V_O^0, with the formation of a $[V_O^0\text{-He}]^0$ complex defect, the interaction energy for He_i and V_O^0 is equal to -4.9 eV, whereas adding more He atoms into V_O^0 results in a postive binding energy (Table 2), implying an unfavorable configuration. Similar results can be obtained for the $[O_i^{2-}\text{-He}]^{2-}$ complex in α-Al_2O_3. These negative binding energies suggest that only a He atom will be trapped by V_O^0 and O_i^{2-}. In summary, He has a larger possibility to cluster themselves in the presence of negatively charged Al cation vacancies. A similar conclusion has been reached in Y_2O_3 from DFT [23].

Table 2 Binding energy of n helium atoms in α-Al_2O_3

	nHe_i	nHe_{Al}^{3-}	$[V_O^0\text{-}nHe_i]^0$	$[O_i^{2-}\text{-}nHe]^{2-}$
n=1	-	−4.5	−4.9	−3.8
n=2	1.94	−0.88	1.34	2.95
n=3	-	1.12	-	-

The fully relaxed configuration of He_{Al}^{3-}, He-He_{Al}^{3-}, He_i, $[V_O^0\text{-}He]^0$ and $[O_i^{2-}\text{-}He]^{2-}$ in α-Al_2O_3 are shown in Fig.3. The fully relaxed configuration of He_{Al}^{3-} is shown in Fig.3(a). It is clear that the He atom substitutes on the Al site, locating at the point equidistant from three oxygen atoms of the close-packed O layer above V_{Al}^{3-}. The distance between He and oxygen atom are 2.084 Å, as shown in Table 1. With adding a second He atom into V_{Al}^{3-}, the 2th He atom occupies the centre of octahedral site along the *c* axis, forming a dumbbell with a He-He distance of 1.990 Å (Fig.3b). He atom of the He_i configuration (Fig.3c) occupies center of the octahedral site, locating at the point closed to equidistant from six oxygen atoms of two close-packed O layers of the octahedral site, with the He-O and He-Al distances ranging from 2.049 Å to 2.051 Å and from 1.918 Å to 2.021 Å respectively (Table 1). For $[V_O^0$-

He$_i$]^0 complex, as shown in Fig.3(d), He atom also occupies the octahedral site along the *c* axis, but locating at the point unequidistant from oxygen atoms of the two close-packed O layers. The O-He and Al-He distances vary within 2.041–2.110 Å and 1.949–2.029 Å respectively (Table 1). Similarly, He atom in [O_i^{2-}-*He*]$^{2-}$ complex occupies the octahedral site, locating at the point unequidistant from oxygen atoms of the two close-packed O layers (Fig.3e), with the O-He and Al-He distances varying within 1.885–2.169 Å and 1.949–1.954 Å respectively (Table 1).

As shown in Fig,3, after relaxation, He relaxes to the nearest OIS from V_O^0 and O_i^{2-} site, resulting in almost same volume occupied by He of *He*$_i$, [V_O^0-*He*$_i$]^0 and [O_i^{2-}-*He*]$^{2-}$. As a result, the He formation energies are nearly equal at the OIS, $V_O^0$and O_i^{2-} positions. Thus, He atom favors to occupy Al vacancies, centers of OIS or form a dumbbell around the Al vacancies, which is in agreement that He prefers to occupy cation vacancy site with large volume and low charge density, while it relaxes to the nearest interstitial site from anion vacancy site owing to a high density of anion vacancy site and its repulsion with full-filled electron shell of He[21].

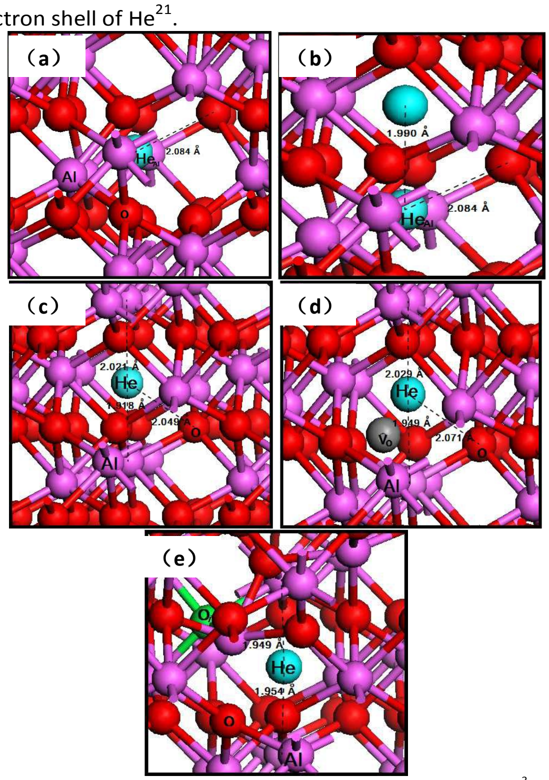

Fig.3 Local structures of a He-related defect in α-Al_2O_3 showing the He_{Al}^{3-}(a), He-He_{Al}^{3-}(b), He_i (c), [V_O^0-He_i]^0 (d) and [O_i^{2-}-He]$^{2-}$(e). Green and blue ball depict oxygen and helium atom respectively

All frequencies identified in Table 1 are real, suggesting these positions as local energy minimum states for He-related defect.

In a word, He atom favors to occupy Al vacancies, centers of OIS or form a dumbbell around the Al vacancies. Furthermore, it has found that the relative stability of intrinsic point defects, under Al-rich conditions, of α-Al_2O_3 is V_{Al}^{3-} > V_O^0 > O_i^{2-} > Al_i^{3+} at the Fermi level[12]. Thus, it can be speculated that imperfect α-Al_2O_3 can act as sinks for trapping He atoms induced by tritium decay or (n, a) reaction irradiation.

3.2 Diffusion of He-related defects in α-Al_2O_3

Having analyzed the formation energies of He related defects, we further investigated *He*$_i$, *He*$_{Al}^{3-}$, [V_O^0-*He*$_i$]^0 and [O_i^{2-}-*He*]$^{2-}$ mobility by calculate the total energy of the defect moving in the paths from one possible site to an adjacent one.

For *He*$_i$, the diffusion from an octahedral interstitial site to an adjacent one (OIS→TS→OIS) was considered. The migration OIS→TS→OIS has a barrier of 2.59 eV (Fig.4), in agreement with the barrier of 2.6 eV calculated from the framework of the polarizable point-ion shell model developed for α-Al_2O_3[14], which show that such diffusion can occur at high temperature. Since positions of octahedral interstitials possess a screw symmetry, such diffusion of He occurs along the c axis simultaneously moving around it. At the saddle point of path OIS→TS→OIS, three real frequencies for the adsorbed He at 874.32 cm^{-1}, 1076.78 cm^{-1}, 1502.73 cm^{-1} and one imaginary frequency at 435.04 cm^{-1} are found. At the starting point, the He$_i$ has a frequency at 933.45 cm^{-1}. At the final point, the He$_i$ has a frequency at 934.63 cm^{-1}, respectively.

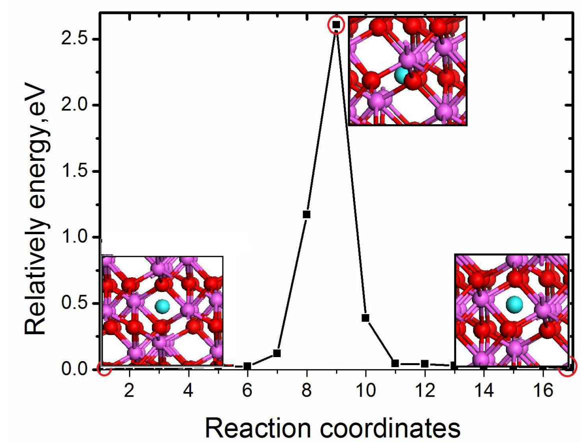

Fig.4 The energy profiles for the migration of He$_i$ in α-Al_2O_3

The minima migration barriers are calculated to be 5.18, 5.98 and 8.52 eV respectively for *He*$_{Al}^{3-}$, [V_O^0-*He*$_i$]^0 and [O_i^{2-}-*He*]$^{2-}$. The relatively high barriers, combined with the formation energies of *He*$_{Al}^{3-}$ and [V_O^0-*He*$_i$]^0 respectively, suggest that incorporation of He-related defects is impossible at the temperatures, probed in the TPB working conditions, of 773–973 K, that is, these defects remain isolable. However, Table 2 demonstrates the thermodynamic feasibility of He trapped by V_{Al}^{3-}, V_O^0 and O_i^{2-}, thus, we calculated the kinetic processes for such trapping respectively.

For V_{Al}^{3-}, the barriers of He diffusion into a V_{Al}^{3-} are characterized by moving the He$_i$ from one of three OIS sites around the V_{Al}^{3-}: (1)OIS,1→V_{Al}^{3-}, (2)OIS,2→V_{Al}^{3-}, (3)OIS,3→V_{Al}^{3-}, (4)OIS,4→OIS,1. Sites OIS,1, OIS,2, OIS,3 and OIS,4 are illustrated in Fig.2. The calculated results show that the barriers are respectively 0.25 eV along the path OIS,1→V_{Al}^{3-} (Fig 5), 1.22 eV on the path OIS,2→V_{Al}^{3-} and 1.16 eV on the path OIS,3→V_{Al}^{3-}. Moreover, the direct-diffusion barrier of He$_i$ are reduced to 1.65 eV from OIS,1 to OIS,2, 1.56 V from OIS,1 to OIS,3 and 2.44 eV from OIS,4 to OIS,1 respectively, compare to the direct-diffusion barrier of He_i in perfect α-Al_2O_3.

Similarly, the barriers of He diffusion into a V_O^0 are characterized by moving the He_i from one of three OIS sites(OIS,2, OIS,3 and OIS,4 illustrated in Fig.2) surrounding the $[V_O^0\text{-}He_{OIS,1}]^0$. The calculated results show that the barriers are respectively 2.05 eV along the path OIS,2→$[V_O^0\text{-}He_{OIS,1}]^0$ (Fig 5), 2.51 eV on the path OIS,3→$[V_O^0\text{-}He_{OIS,1}]$ and 2.65 eV on the path OIS,4→$[V_O^0\text{-}He_{OIS,1}]^0$. The calculated results for the path OIS,2→$[V_O^0\text{-}He_{OIS,1}]^0$ and the path OIS,3→$[V_O^0\text{-}He_{OIS,1}]$ are still lower than the direct-diffusion barrier of He_i. However, the barriers of He diffusion into a O_i^{2-} from one of three surrounding OIS sites (OIS,2, OIS,3 and OIS,5 illustrated in Fig.2) vary with in 3.05–3.26 eV, higher than the direct-diffusion barrier of He_i.

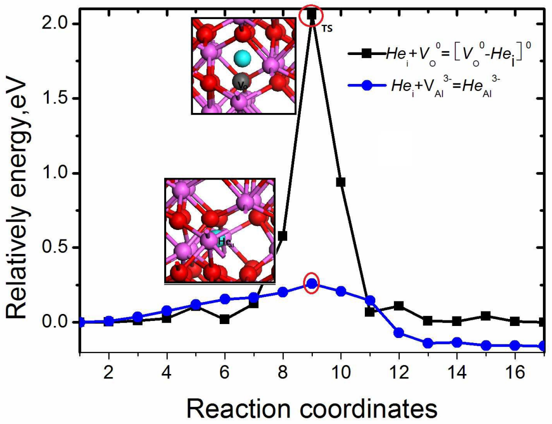

Fig.5 The energy profiles for He_i trapping by V_{Al}^{3-} and V_O^0 in α-Al_2O_3

Thus, He_i is more likely diffusion into V_{Al}^{3-} and V_O^0 than the direct diffusion with path OIS→OIS, suggesting that He trapped by V_{Al}^{3-} or V_O^0 is thermodynamically and kinetically feasible, away from the V_{Al}^{3-} and V_O^0, He jumps from one OIS to another with a barrier of 2.59 eV. So while it is energetically more favourable for He to be in V_{Al}^{3-} or V_O^0, a significant energy barrier exists for OIS→OIS diffusion. In other word, it is possible that at finite temperatures a number of events involve He diffusion into V_{Al}^{3-} or V_O^0 before migration along the *c* axis from one OIS to another takes place. Therefore, the hydrogen interactions with He_i, He_{Al}^{3-}, and $[V_O^0\text{-}He_i]^0$ will be focused in next section.

3.3 He-related defects interaction with H in α-Al_2O_3

To see He-related defects interaction with H, one H atom is set into He_i, He_{Al}^{3-} and $[V_O^0\text{-}He_i]^0$, respectively. The formation energy of H-He complex defects ($E_f^{H,He}$) can be obtained by

$$E_f^{H,He} = E_{H-He-related-defect} - (E_{He-related-defect} + \frac{1}{2}E_{H_2}) \quad (3)$$

, where $E_{H-He-related-defect}$ and $E_{He-related-defect}$ are the total energy of the He-related defect system with and without H atom, respectively. E_{H_2} is the energy of a H_2 molecule. The energy of H_2 molecule is calculated to be -31.794 eV, with a H-H band of a 0.749 Å and a vibrational frequency of 4385.6 cm^{-1},which agree reasonably well the experimental result of 4395.5 cm^{-1}[24].

The formation energies and optimized geometries of H-He complex defects in α-Al_2O_3 have been summarized in Table 3. Interestingly, it can be seen from Table 3 that $[He_{Al}^{3-}\text{-}H^+]^{2-}$ and $[H_O^+\text{-}He_i]^+$ have negative formation energies, denoting such H-He complex defects are more stable than the gas phase H_2, which suggest that such H-He complex defects will be formed spontaneously. However, $[He_i\text{-}H^+]^+$, having positive formation energy, will be formed unspontaneously, meaning it is unstable and will decay.

Combined with formation energies for H-related defects in bulk α-Al_2O_3 without He [12], the binding energy between H_i^+ and He_{Al}^{3-} is negative for $[He_{Al}^{3-}\text{-}H^+]^{2-}$ defect (Table 3), signifying that H_i^+ atom and He_{Al}^{3-} tend to attract each other, which suggests the H_i^+ will be trapped by the He_{Al}^{3-}. Similar results can be obtained for $[H_O^+\text{-}He_i]^+$ and $[He_i\text{-}H^+]^+$ complexes in α-Al_2O_3(Table 3). For trapping of a proton by $[V_O^0\text{-}He_i]^0$ defect, with the formation of a $[H_O^+\text{-}He_i]^+$ complex, the binding energy for H_i^+ and $[V_O^0\text{-}He_i]^0$ is equal to -4.05 eV. The binding energy for trapping of a proton by He_i, with formation of a $[He_i\text{-}H^+]^+$ complex in the energy favorable configuration, is equal to -0.86 eV. These negative binding energies suggest that the H_i^+ will be trapped by the He_{Al}^{3-}, $[V_O^0\text{-}He_i]^0$ and He_i, increasing the activation energy of H migration and decreasing the H mobility. This is favored for low H-transport in α-Al_2O_3 TPB.

Having a negative binding energy, however, does not mean that these complexes will readily form. Under thermal equilibrium, the binding energy needs to be greater than the larger of formation energy for the complex to have higher concentration than its constituents [22]. Comparing with the formation energies of H [12] and He (Table1) related defects respectively, we can find the binding energy of $[He_{Al}^{3-}\text{-}H^+]^{2-}$ and $[H_O^+\text{-}He_i]^+$ are larger than both formation energies of their constituents, while that of $[He_i\text{-}H^+]^+$ is smaller than the larger their constituents, suggesting that H_i^+, $[V_O^0\text{-}He_i]^0$ and He_{Al}^{3-} are likely to exist in the form of $[He_{Al}^{3-}\text{-}H^+]^{2-}$ and $[H_O^+\text{-}He_i]^+$, whereas H_i^+ and He_i are likely to exist in the form of $[He_i\text{-}H^+]^+$, but also in isolated point defects. However, the dominant defects of He-H complexes will predicted according to formation energies at the Fermi level, with studies of chemical potentials of H-He complexes. This is urgent to be determined in future.

Table3 Formation energy E_f , Binding energy E_b, O-H distance d_{O-H}, Al-H distance d_{Al-H}, O-He distance d_{O-He}, Al-He distance d_{Al-He}, H frequencies(ω_H) and He frequencies(ω_H) of H-He complexes in α-Al_2O_3, with ZPE values shown in parentheses

Configuration	$[He_{Al}^{3-}\text{-}H^+]^{2-}$	$[He_i\text{-}H^+]^+$	$[H_O^+\text{-}He_i]^+$
E_f (eV)	-3.11 (0.098)	0.28 (0.116)	-3.00 (0.067)
E_b(eV)	−3.11	−0.86	−4.05
$d_{O\text{-}H}$ (Å)	0.980	0.989	2.520–3.825
$d_{He\text{-}H}$(Å)	1.339	1.389	1.856
$d_{O\text{-}He}$ (Å)	2.060–2.150	1.937–2.101	2.037–2.200
$d_{Al\text{-}He}$(Å)	2.571–4.779	2.031–2.134	1.986–2.119
ω_H(cm^{-1})	1079.26,3536.38	1023.1,1382.76, 3245.18	1010.92, 1171.34, 1298.76
ω_{He}(cm^{-1})	863.61,877.82	901.44, 956.12	906.43

The fully relaxed configuration of $[He_{Al}^{3-}\text{-}H^+]^{2-}$, $[He_i\text{-}H^+]^+$ and $[H_O^+\text{-}He_i]^+$ are shown in Fig.6. A proton can bind to one of six nearest neighbor oxygen atoms of the octahedral site in the Al sublattice with a He_{Al}^{3-} occupying, pointing toward the vacancy center, and forming a $[He_{Al}^{3-}\text{-}H^+]^{2-}$ complex (Fig.6a). The $[He_{Al}^{3-}\text{-}H^+]^{2-}$ has a fully relaxed O-H bond length of 0.980 Å (Table 3), in well agreement with that of the case without He [12] and the experimentally O-H bond in H_2O[24] respectively. As compared to that of He_{Al}^{3-} (Table2), the O-He distances of $[He_{Al}^{3-}\text{-}H^+]^{2-}$ complex either increase or decrease, which is reflected by the increase and decrease of the O-He distances from 2.084 Å to 2.150 Å and from 2.084 Å to 2.060 Å respectively.

The H^+ is localized to one of six nearest neighbor oxygen atoms of the octahedral site with a He_i occupying, pointing toward the vacant, as shown in Fig.6(b). It is found that the O-H bond distance of 0.989 Å (Table 3) is slightly smaller that of the case without He_i [12] and but longer than the O-H bend length of H_2O [24]. When H^+ is introduced, the increase and decrease of the O-He distances vary from 2.051 Å to 2.101Å and from 2.049 Å to 1.937 Å, and the increase in the Al-He distances is 0.113 Å (Table 3) respectively, comparing with that of He_i in bulk Al_2O_3.

The fully relaxed configuration of $[H_O^+\text{-}He_i]^+$ is shown in Fig.6(c). It is found that H substitutes on the O site, locating in the basal plane of oxygen atoms, and He occupies the octahedral site, with the O-He and Al-He distances increasing by 0.009Å and 0.019–0.104 Å respectively.

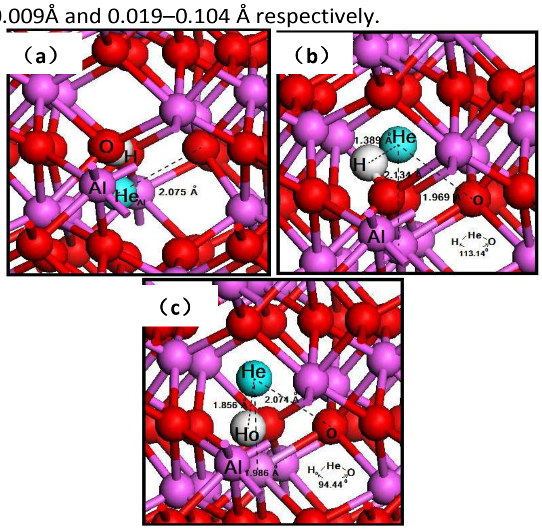

Fig.6 Local structures of H-He complex defect in α-Al_2O_3 showing the $[He_{Al}^{3-}\text{-}H^+]^{2-}$ (a), $[He_i\text{-}H^+]^+$(b) and $[H_O^+\text{-}He_i]^+$(c), white ball depict hydrogen atom.

Table 3 also shows that the calculated vibrational frequencies of the O-H stretching mode in α-Al_2O_3, similar to the typical O-H stretch frequencies [24].

In summary, in presence of He, forms of H related defect in α-Al_2O_3 with intrinsic point defects presenting, are He_i, H_i^+, $[He_i\text{-}H^+]^+$, $[He_{Al}^{3-}\text{-}H^+]^{2-}$ and $[H_O^+\text{-}He_i]^+$. Thus, a proton favors lattice oxygen O_x and O vacancies of α-Al_2O_3 with He presence, similar to the typical H-configuration in bulk Al_2O_3.

3.4 H diffusion into He-related defects in α-Al_2O_3

In view of thermodynamics, the above results suggest that H_i^+ can be trapped by the He_{Al}^{3-}, He_i and $[V_O^0\text{-}He_i]^0$, which will increase activation energy of H migration. However, to fully elucidate how H_i^+ diffuses into He related defects, the migration of H atoms should be explored.

In case of bulk α-Al_2O_3 without He, we have found that diffusion of H_i^+ occurs along the c axis from an octahedral site to an adjacent one (OIS→TS→OIS), with a barrier of 1.26 eV [12]. Away from the He_i, He_{Al}^{3-} and $[V_O^0\text{-}He_i]^0$, H_i^+ also jumps from one OIS to another with the same diffusion barrier for H_i^+ in perfect α-Al_2O_3. As closed to He-related defects, we mainly considered H diffusion into and out of He_i, He_{Al}^{3-} and $[V_O^0\text{-}He_i]^0$ respectively: (1) moving the H_i^+ step by step from OIS,4 to first adjacent OIS,1 with a He_i, and then to second adjacent OIS,2; (2) from OIS,4 to first adjacent OIS,1 with a He_{Al}^{3-}, and then to second nearest OIS,2; (3) from OIS,4, OIS,3 and OIS,5 to first adjacent OIS,1 with $[V_O^0\text{-}He_i]^0$. Sites OIS,1, OIS,2, OIS,3, OIS,4 and OIS,5 are illustrated in Fig.2.

For He_i presence, the calculated results show that the barriers is 1.28 eV along the path OIS,4→TS→OIS,1(Fig.7), close to 1.26 eV for case without He_i. The reversed path, OIS,1→TS→OIS,4, proceeds in an exothermic fashion with a smaller energy barrier of 0.76 eV. Similarly, the H_i^+ diffusion barrier is reduced to 1.18 eV from OIS,1 to OIS,2. Thus, it is definitely easier for dissociation of $[He_i\text{-}H^+]^+$ than H_i^+ diffusion into He_i. It can be seen from Fig.7 that the energy profiles of the path OIS,4 → OIS,1 show that H_i^+ migrates in a similar fashion in perfect α-Al_2O_3, involving two steps: (1) the reorientation step in which the hydrogen atom remains bonded to the same oxygen atom (IS→state9→state10) and (2) the hopping step in which breaking and reforming of the O-H bond takes place (state12→state13→FS). At the saddle point of path OIS,4→TS→OIS,1, real frequencies for the adsorbed H_i^+ at 1432.29 and 3756.01 cm^{-1}, and He_i at 889.95, 944.88 cm^{-1}, with one imaginary frequency at 795.57 cm^{-1}, are found. At the final point, the frequencies of H_i^+ and He_i are shown in Table 3. At the starting point, the H_i^+ has two frequencies at 1237.68, 3067.61, cm^{-1}, the He_i has two frequencies at 917.40 and 943.49 cm^{-1}, respectively.

In presence of He_{Al}^{3-}, the direct-diffusion barrier of H_i^+ are reduced to 0.39 eV from OIS,4 to OIS,1 and 0.82 V from OIS,1 to OIS,2, respectively, compare to that of the case without He_{Al}^{3-}. The reversed path, OIS,1→TS→OIS,4, proceeds in a endothermic fashion with a higher energy barrier of 2.52 eV. Thus, we can conclude that H_i^+ diffusion into He_{Al}^{3-} is definitely easier than dissociation of [He_{Al}^{3-}-H^+]$^{2-}$. The energy profiles of the path OIS,4→TS→OIS,1show that H_i^+ migrates into He_{Al}^{3-} also involves the two steps, as shown in Fig.7. At the saddle point of path OIS,4→TS→OIS,1, two real frequencies for the adsorbed H_i^+ at 1271.90 and 3180.28 cm^{-1}, and three real frequencies for the He_{Al}^{3-} at 867.56, 878.9 and 882.85 cm^{-1}, with one imaginary frequency at 429.12 cm^{-1}, are found. At the final point, the frequencies of H_i^+ and He_{Al}^{3-} are shown in Table 3. At starting the point, the H_i^+ has two frequencies at 1138.19 and 3332.58 cm^{-1}, the He_i has three frequencies at 878.92, 885.48 and 898.08 cm^{-1}, respectively.

Similarly, H_i^+ diffusion into [V_O^0-He_i]^0 is easier than dissociation of [H_O^+-He_i]$^+$. The barriers are respectively 1.28 eV along the path OIS,4→OIS,1(Fig.7), 1.97 eV on the path OIS,5→OIS,1 and 1.94 eV on the path OIS,4→OIS,1. The reversed path, OIS,1→TS→OIS,4, proceeds with a larger energy barrier of 4.58 eV. The energy profiles of the path OIS,4→OIS,1 shows that H_i^+ migrates into [V_O^0-He_i]^0 by breaking of the O-H bond following by the hydrogen atom hopping into V_O. At the saddle point of path OIS,4→TS→OIS,1, three real frequencies for the adsorbed H_i^+ at 874.32 cm^{-1}, 1076.78 cm^{-1}, 1502.73 cm^{-1} and one imaginary frequency at 435.04 cm^{-1} are found. At the final point, the frequencies of Ho^+ and He_i are shown in Table 3. At the final starting point, the H_i^+ has a frequency at 933.45 cm^{-1}, the [V_O^0-He_i]^0 has three frequencies at 933.63 cm^{-1}, respectively.

In summary, dissociation of [He_i-H^+]$^+$ is kinetically more feasible, whereas H_i^+ trapping by the He_{Al}^{3-} and [V_O^0-He_i]^0 are thermodynamically and kinetically feasible. Thus, H atoms in bulk α-Al_2O_3 can be in present of He_i, H_i^+, [He_i-H^+]$^+$, [He_{Al}^{3-}-H^+]$^{2-}$ and [H_O^+-He_i]$^+$ due to He existence, in good agreement with thermodynamics results.

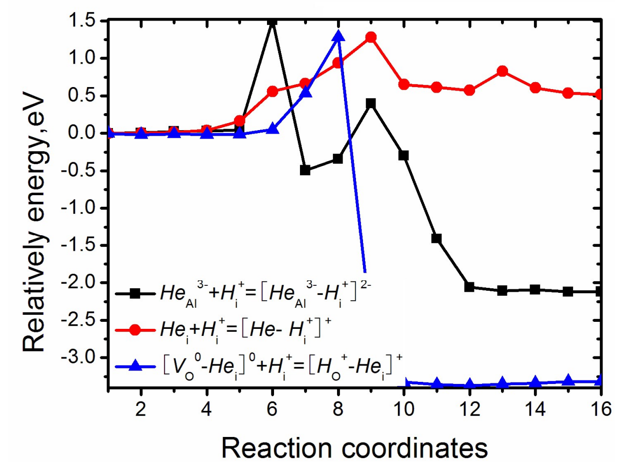

Fig.7 The energy profiles for the H_i^+ trapping by He_i , He_{Al}^{3-} and [V_O^0-He_i]^0 in α-Al_2O_3

In additional, it can be inferred that He_{Al}^{3-} and [V_O^0-He_i]^0 presenting in α-Al_2O_3 will increase the activation energy of H migration, decreasing the H mobility, which is favored for low H-transport in α-Al_2O_3 TPB. However, the sharply increased He_{Al}^{3-} and [V_O^0-He_i]^0 would lead to a more brittle, which requires particular attention. Without the required ductility to allow blistering, α-Al_2O_3 as TPB can experience significantly increased cracking, which will lead to the hydrogen gas to directly contact the underlying metal surface of α-Al_2O_3 TPB. Thus, proper concentration of defects forming in α-Al_2O_3 TPB is urgent to be determined in future.

4. Conclusions

Helium behavior and its interactions with H in α-Al_2O_3 are studied under H_2-rich conditions from density functional theory (DFT). Our results indicate that He atom favors to occupy Al vacancies, centres of OIS or form a dumbbell around Al vacancies, forming He_i, He_{Al}^{3-}, He_i-He_{Al}^{3-},[V_O^0-He_i]^0 and [O_i^{2-}-He]$^{2-}$complexes, among of which He_{Al}^{3-} forms most readily. At finite temperatures a number of events involve He diffusion into V_{Al}^{3-} or V_O^0 before migration along the *c* axis from one OIS to another takes place. Two He atoms can be trapped by the V_{Al}^{3-}, whereas only a He atom trapped by OIS, V_O^0 and O_i^{2-}, thus He atom has a larger possibility to cluster themselves around the negatively charged Al cation vacancies, inducting that imperfect α-Al_2O_3 can act as sinks for trapping He atoms induced by tritium decay or (n, a) reaction irradiation.

With He presence, a proton still prefer to occupy lattice oxygen O_x and O vacancies of α-Al_2O_3, similar to the typical H-configuration in bulk Al_2O_3. H_i^+ trapping into the He_{Al}^{3-} and [V_O^0-He_i]^0 are thermodynamically and kinetically feasible, whereas dissociation of [He_i-H^+]$^+$ is feasible. He_{Al}^{3-} and [V_O^0-He_i]^0 presenting in α-Al_2O_3 will increase the activation energy of H migration, decreasing the H mobility, which is favored for low H-transport in α-Al_2O_3 TPB. Forms of H,He related defect in α-Al_2O_3 are He_i, H_i^+, [He_i-H^+]$^+$, [He_{Al}^{3-}-H^+]$^{2-}$and [H_O^+-He_i]$^+$, but determination of the dominant defects with formation energies at the Fermi level requires further calculations including chemical potentials of H-He complexes.

Acknowledgements

This work is supported by National Magnetic Confinement Fusion Science Program (No.2013GB110006B) and National Natural Science Foundation (No.21471137, 11275175) of China.

Notes and references

1 K. Hashizume, K. Ogata, M. Nishikawa, T. Tanabe, S. Abe, S. Akamaru and Y. Hatano, *J.Nucl.Mater.*, 2013,442: S880.
2 G.W.Hollenberg, E.P.Simonen, G.Kalinin and A.Terlain. *Fusion Eng.Des.*,1995,28,190.
3 A.Causey Rion, A.Karnesky Richard and San.Marchi Chris, *Comprehensive Nucl. Mater.*, 2012, 4, 511.
4 X.Xiang, X.Wang, G.Zhang, T.Tang and X.Lai, *Int. J. Hydrogen Energy*, 2015, 40: 3696.
5 K.Arshak and O.Korostynska, *Mater. Sci.Eng.B*, 2006, 133, 1
6 P.Trocellier, S.Agarwal and S.Miro, *J.Nucl.Mater.*,2013, 445:128
7 M. Katsuyuki, T. Tomohito, Y .Takahisa and I.Yuichi, *Phys. Rev. B*, 2003, 68,085110
8 X.Xiang, G.Zhang, X.Wang, T.Tang and Y.Shi, *Phys. Chem. Chem. Phys.*, 2015, 17, 29134

9 A.B.Belonoshko, A.Rosengren, Q.Dongm, G.Hultquist and C.Leygraf, *Phys. Rev.B*, 2004, 69,24302
10 W. Mao, C. Takumi, S. Kenichiro, A. Suzuki and T. Terai , *Fusion Eng. Des.*, 2013, 28,190
11 Aaron.M. Holder, Kevin D. Osborn, C. J. Lobb and Charles B, *Phys. Rev. Lett.*, 2013, 111,065901
12 G. Zhang, Y Lu and X.L.Wang,*Phys. Chem. Chem. Phys.*, 2014, 16,17523.
13 C.Filleux, M. Morgeli, W. Stetller, P. Eberhardt and J. Geiss, *Rad. Eff.,*1980,46,1.
14 D. O. Welch, O. Lazaretha, G. J. Dienes and R. D. Hatcher. *Rad. Eff.,*1976,28,195.
15 B.Delley, *J. Chem.Phys.*, 2000, 113, 7756
16 J.A.White and D.MBird, *Phys.Rev.B*, 1994, 50, 4954
17 J.P.Perdew, K.Burke and M.Ernzerhof, *Phys.Rev.Lett.,*1996,77, 3865
18 B.Delley, *J. Chem. Phys.*, 1990, 92,508.
19 T. van Mourik and J.H. van Lenthe, *J. Chem. Phys.,* 1995,102,7479.
20 D.M. Ceperley and H. Partridge, *J. Chem. Phys.*, 1986,84, 821.
21 M.J.Puska, R.M.Nieminen and M.Manninen, *Phys.Rev.B*, 1991, 23 (6): 3037.
22 J.B.Varley, H.Peelaers, A.Janotti and C.G.Van de Walle, *J. Phys: Condens Matter*, 2011, 23, 334212
23 Y.D.Ou and W.S.Lai, *Nucl. Instrum. Methods Phys. Res. B*,2011,269:1720.
24 K.P.Huber, G.Hertzberg, Molecular spectra and molecular structure IV: Constants of diatomic molecules, New York: Van Norstrand Reinhold, 1979,300.